ChemComm

COMMUNICATION

View Article Online
View Journal | View Issue

Cite this: *Chem. Commun.*, 2021, **57**, 11673

Received 24th September 2021,
Accepted 12th October 2021

DOI: 10.1039/d1cc05408b

rsc.li/chemcomm

Alumination of aryl methyl ethers: switching between sp^2 and sp^3 C–O bond functionalisation with Pd-catalysis†

Ryan K. Brown,‡[a] Thomas N. Hooper,‡[a] Feriel Rekhroukh,‡[b] Andrew J. P. White,[a] Paulo J. Costa[b] and Mark R. Crimmin*[a]

The reaction of [{(ArNCMe)$_2$CH}Al] (Ar = 2,6-di-iso-propylphenyl) with aryl methyl ethers proceeded with alumination of the sp^3 C–O bond. The selectivity of this reaction could be switched by inclusion of a catalyst. In the presence of [Pd(PCy$_3$)$_2$], chemoselective sp^2 C–O bond functionalisation was observed. Kinetic isotope experiments and DFT calculations support a catalytic pathway involving the ligand-assisted oxidative addition of the sp^2 C–O bond to a Pd–Al intermetallic complex.

Lignin from lignocellulosic biomass is derived from a radical polymerisation of monolignols (*p*-coumaryl, coniferyl, and sinapyl alcohol) and its composition varies from *genus* to *genus*.[1–3] The depolymerization of lignin has gained significant attention over the last 10 years, and while there is a breadth of research in this area, a clear finding of this work is that the products of depolymerization are often structurally related to monolignols themselves.[4] Many of these depolymerisation products contain aryl methyl ether moieties.[5–7] One example of a product made directly from lignin is vanillin, which is widely used in commercial applications (Fig. 1).[8]

Despite the importance of aryl methyl ethers as sustainable chemical building blocks, reactions that break the strong C–O bonds in these substrates are rare,[9] those which form reactive fragments amenable for synthetic diversification are rarer still. For example, nickel catalysed silylation reactions of sp^2 C–O bonds have been pioneered by Martin and coworkers with initial reactions focussing on silylation of aryl and benzyl pivalates with a silyl-borane reagent.[10,11] This was later expanded to include aryl, benzyl and vinyl ethers.[12] The nickel catalysed stannylation of C–O bonds of aryl esters with a silyl stannane has also been reported using a similar protocol.[13] Related reactions with boron reagents are known. Chatani and coworkers have reported the Rh catalysed borylation of pyridyl ethers,[14] while Martin and co-workers have used diboranes to borylate aryl and vinyl ethers in the presence of a nickel catalyst.[15] Very recently, Nakao and coworkers reported the borylation of methyl aryl ethers using a heterometallic Rh–Al complex.[16] Despite these important examples, most studies to date have focused on derivatives of phenol, in the case of aryl methyl ethers the substrate of choice is anisole. Application of this type of methodology to electron-rich and *ortho*-substituted motifs, such as 1,2-dimethoxybenzene, remains uncommon.

Monolignol derivatives are structurally complex and potentially contain multiple adjacent sp^2 C–O and sp^3 C–O bonds in the same molecule. A particular challenge in this area of research is controlling chemoselectivity. The bond dissociation energies of the sp^2 C–O bond of phenyl methyl ether is 101 ± 1 kcal mol^{-1} while the sp^3 C–O bond of dimethyl ether is 83.2 ± 0.9 kcal mol^{-1}.[17] In this paper, we report a method for the transformation of C–O bonds of aryl methyl ethers into C–Al bonds. The work builds on an established program from our lab focusing on main group reagents for C–O bond activation.[18–20] We show that the chemoselectivity of the reaction can be precisely controlled through inclusion or exclusion

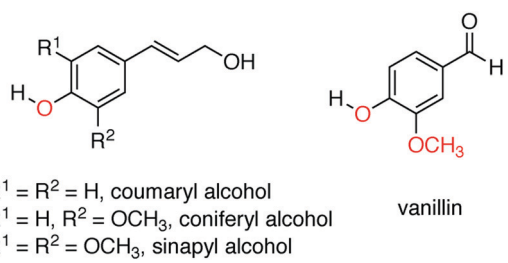

$R^1 = R^2 = H$, coumaryl alcohol
$R^1 = H$, $R^2 = OCH_3$, coniferyl alcohol
$R^1 = R^2 = OCH_3$, sinapyl alcohol

vanillin

Fig. 1 Monolignols (building blocks for lignin) along with vanillin.

[a] *Department of Chemistry, Molecular Sciences Research Hub, Imperial College London, 82 Wood Lane, Shepherds Bush, London, W12 0BZ, UK. E-mail: m.crimmin@imperial.ac.uk*
[b] *BioISI – Biosystems & Integrative Sciences Institute, Faculty of Sciences, University of Lisboa, 1749-016 Lisboa, Portugal*

† Electronic supplementary information (ESI) available: Experimental procedures, details of calculations and characterization data (PDF). Coordinates for DFT calculations (*xyz*). Crystallographic data for **3a**, **3c**, **4a**, **4b**, and **4d** (*cif*). CCDC 1973118–1973121. For ESI and crystallographic data in CIF or other electronic format see DOI: 10.1039/d1cc05408b

‡ These authors contributed equally and are listed in alphabetical order.

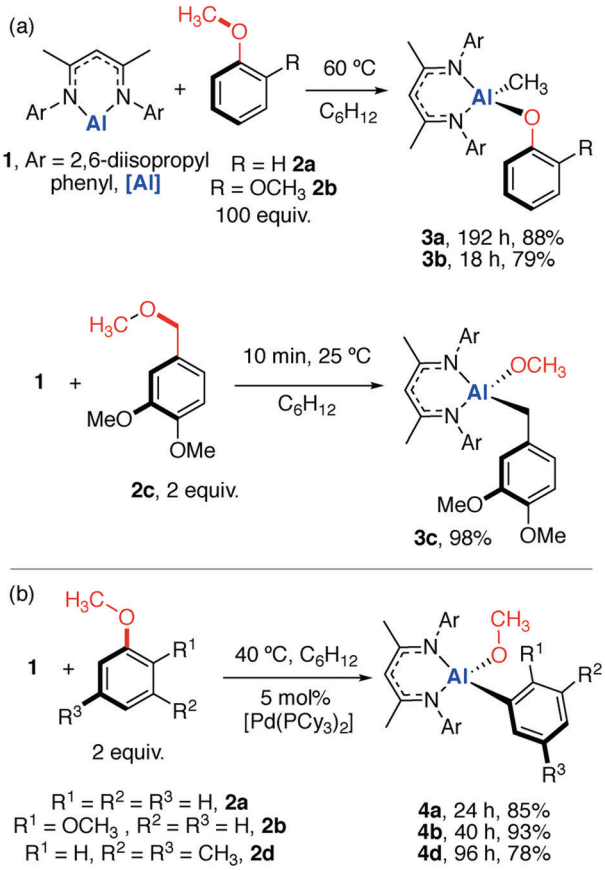

Scheme 1 (a) Non-catalysed and (b) catalysed reactions of **1** with aryl methyl ethers.

of a homogeneous palladium catalyst, allowing a tuneable approach to either sp^3 C–O bond activation or sp^2 C–O bond activation of aryl methyl ethers.

Anisole and derivatives thereof can be functionalised by reaction with the aluminium reagent **1** (Scheme 1a).[21,22] The non-catalysed reaction of an excess of anisole (**2a**, 100 equiv. or neat) with **1** resulted in cleavage of the sp^3 C–O bond and formation of new Al–CH_3 and Al–OPh functional groups. The reaction is entirely chemoselective and a large excess of anisole is required.[23] Reaction of **1** with 1,2-dimethoxybenzene (**2b**) also resulted in the chemoselective alumination of the sp^3 C–O bond. In contrast, the reaction of **1** with the methyl protected vanillyl alcohol **2c** (derived from vanillin) resulted in the selective reaction of a dialkyl ether moiety to form **3c**, despite the presence of two distinct aryl methyl ether groups. **3a** and **3b** show peaks in the ^{1}H NMR spectrum at $\delta = -0.68$ (s, 3H) and -0.65 ppm (s, 3H) respectively. These high-field resonances are characteristic of Al–CH_3 groups. In contrast, the benzylic CH_2 group of **3c** is considerably more deshielded and resonates at $\delta = 1.46$ ppm in the ^{1}H NMR spectrum. **3a** and **3c** have also been characterised by single crystal X-ray diffraction (Fig. 2).

The non-catalysed reactions of **1** with aryl methyl ethers are consistent with established reactivity patterns of these functional groups. Direct attack of nucleophiles on the CH_3 moiety can occur due to the ability of OPh^- to act as a leaving group. Typically, an S_N2 pathway is invoked to explain this behaviour. Recently a number of aluminyl anions (aluminium based nucleophiles) related to **1** have been shown to effect sp^3 C–O bond alumination of aryl methyl ethers.[24,25]

Notable changes in selectivity and reaction times were observed when the reactions were conducted in the presence of a catalyst. Addition of [$Pd(PCy_3)_2$] (5 mol%) to a mixture of **1** and 2 equiv. of anisole (**2a**) resulted in sp^2 C–O bond functionalisation to form **4a** (Scheme 1b).§ Similarly, 1,2-dimethoxybenzene and 1-methoxy-3,5-dimethylbenzene resulted in clean catalytic reactions with **1** to form **4b** and **4d** respectively. The catalytic protocol occurs under milder conditions than the non-catalysed (40 *vs.* 60 °C) and proceeds with high chemoselectivity for the sp^2 C–O bond of the substrate. **4a–b** and **4d** were characterised by distinct resonances at δ = 3.38 to 3.75 ppm in the ^{1}H NMR spectrum assigned to the –OCH_3 group derived from C–O bond functionalisation. To unambiguously determine their structures **4a–b** and **4d** were also characterised by single crystal X-ray diffraction (Fig. 2). The *ortho*–OCH_3 group in **4b** shows a close contact with aluminium centre; the Al–O2 bond length is ~3.0 Å and within the sum of the van der Waals radii (3.36 Å).[26]

We have previously shown the combination of **1** with catalytic [$Pd(PCy_3)_2$] is able to achieve the C–H, C–O and C–F alumination of unactivated arenes, furans, and fluoroarenes under mild conditions. In certain cases, remarkable changes in selectivity have been observed between catalytic and non-catalytic protocols.[19,20,27–29]

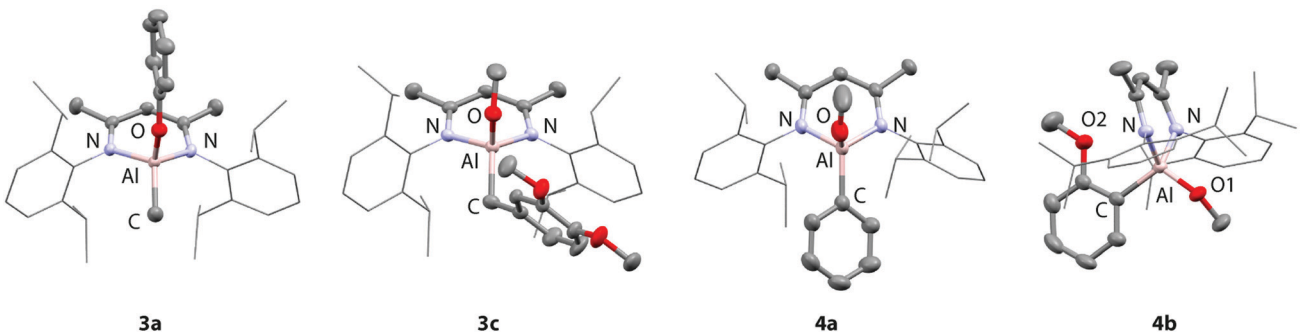

3a **3c** **4a** **4b**

Fig. 2 Structures of **3a**, **3c**, **4a**, and **4b** determined by single crystal X-ray diffraction studies. Hydrogen atoms and components of disorder omitted for clarity. 50% probability ellipsoids. Bond lengths reported in Å.

Others have shown that modification of reagents or conditions can result in switches in selectivity between the functionalisation of sp^2 and sp^3 C–O bonds with Ni-based catalysts.[15,30]

To shed further light on the mechanisms of C–O bond activation and the switch in selectivity, further experiments and calculations were undertaken. The non-catalysed reaction of **1** with **2a** was presumed to occur by an S_N2 mechanism in which **1** acts as an aluminium-centered nucleophile.[31,32] Under pseudo-first order conditions (excess anisole), kinetics data could be fitted to 1st order in [**1**] across a series of initial concentrations. Competition experiments between anisole (**2a**), 1,2-dimethoxybenzene (**2b**) and **1** revealed that the latter substrate reacts fastest. This finding is consistent with the established Lewis-acidity of **1** and indicates the *ortho*-methoxy moiety can act as a directing group. DFT calculations suggest that the S_N2 pathway is not only plausible, but also potentially facilitated by general base catalysis and/or Lewis-acid catalysis (see ESI† for further details).

Given the switch in selectivity under catalytic conditions, it is highly likely an alternative mechanism is in operation in the presence of $[Pd(PCy_3)_2]$. A series of plausible pathways for the reaction of $[Pd(\mathbf{1})_2]$[28,29] were investigated by DFT calculations. The lowest energy calculated pathway involves the ligand-assisted oxidative addition of the sp^2 C–O bond of anisole to $[Pd(\mathbf{1})_2]$ and leads directly to a Pd-coordinated analogue of **4a** (Fig. 3). Approach of anisole to $[Pd(\mathbf{1})_2]$ forms **Int-1** which involves a weak interaction between Pd and the π-system of anisole through the C_{ipso}–O bond. The potential formation of transition metal π-complexes as unstable intermediates in the C–O bond functionalisation of aryl esters, aryl carbamates, aryl sulfamates, and aryl ethers has been highlighted previously.[33–35] **Int-1** evolves to **Int-2** by **TS-1** and this step leads to the coordination of the oxygen lone pair to the 3p orbital of one of the aluminylene ligands of the $[Pd(\mathbf{1})_2]$ fragment with synchronous interaction of the electron-rich Pd centre with the sp^2 C atom. **Int-2** is the precursor for the ligand assisted oxidative addition step. Activation and breaking of the sp^2 C–O bond occurs by **TS-2** and this is the highest barrier on the pathway $\Delta G^{\ddagger}$ = 15.5 kcal mol^{-1}. The coordinated reaction product **Int-3** is generated directly from **TS-2** with migration of both the CH_3 and OPh fragments to Al occurring in this step. Across the sequence **Int-1**–**TS-1**–**Int-2**–**TS-2**–**Int-3** the sp^2 C–O bond of anisole stretches from 1.36–1.43–1.47–1.64–3.05 Å, the Wiberg Bond index of the C–O bond decreases from 1.01–0.85–0.79–0.57–0.02, and the NPA charge of the key Al atom increases from 0.99–1.09–0.99–1.39–2.16.

QTAIM calculations return data for a four-membered ring constructed from Pd, C, O and Al atoms for **Int-2**, which is again consistent with a ligand-assisted oxidative addition pathway. Bond paths are found between each atom and a ring critical point located in the centre of the four-membered ring. In addition to the short Al–O distance of 2.15 Å detected in the optimized geometry of **Int-2**, the presence of a primarily ionic interaction between Al and O atoms was evidenced by the attributes of the BCP (ρ = 0.033 e $Bohr^{-3}$, $\nabla^2\rho$ = 0.12 e $Bohr^{-5}$). Further analysis of the QTAIM data is consistent with a strengthening of the Al–O interaction and weakening of the C–O interaction along the reaction coordinate (see ESI†).

Alternative pathways involving either the direct oxidative addition of the sp^2 C–O bond ($\Delta G^{\ddagger}$ = 44.8 kcal mol^{-1}) or the *ortho* sp^2 C–H bond ($\Delta G^{\ddagger}$ = 26.5 kcal mol^{-1}) of anisole to $[Pd(\mathbf{1})_2]$ were calculated to occur with higher energy transition states and would not be expected to be competitive. To further exclude the possibility that the reaction occurs through a mechanism involving C–H bond activation on or before the turnover-limiting step, the kinetic isotope effect (KIE) was determined experimentally. The KIE for the reaction of **2a** and d_8-**2a** was measured by both independent rates (1.3 ± 0.1) and an intermolecular competition experiment (1.2 ± 0.1). The lack of a significant KIE is consistent with a turnover-limiting step that involves the direct cleavage of the C–O bond.

Ligand-assisted oxidative addition has been invoked to explain the reaction of aryl halides with complexes containing M–PR_3,[36] M–SiR_3,[37] and M–BR_2 bonds.[38] Such a pathway has even been considered to explain the assistive role of magnesium reagents in the cross-coupling of fluoroarenes.[39] We proposed that ligand-assisted oxidative addition may be a key

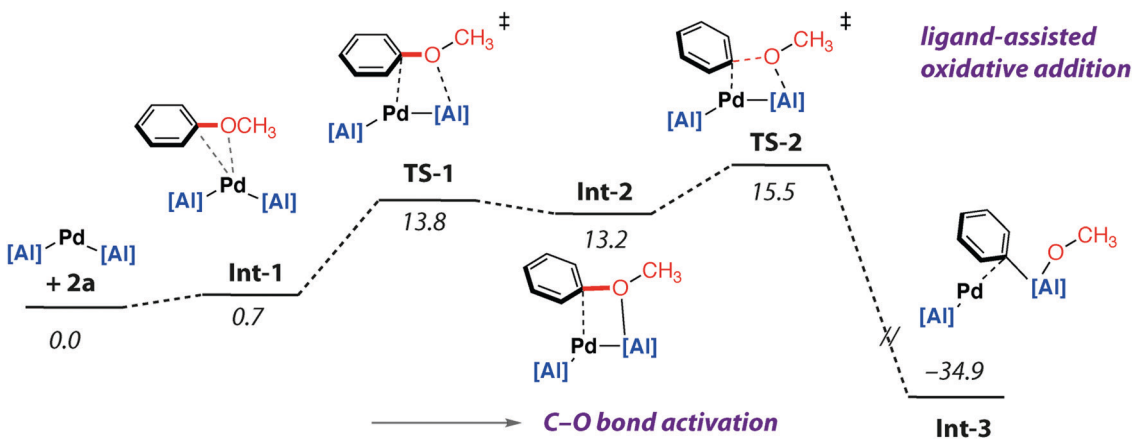

Fig. 3 DFT calculated pathway for the Pd-catalysed reaction of **1** with anisole (**2a**). Gibbs energies in kcal mol^{-1}.

step during the reaction of **1** with fluorobenzene with the same catalyst system reported herein.[27] Ligand-assisted oxidative addition involves a four-membered transition state (rather than a classical three-membered oxidative addition transition state) and is reliant on the ligand acting as an acceptor. There is a clear analogy to Lewis-acid assisted processes and it is notable that a number of reactions involving C–O bond activation of aryl methyl ethers with transition metals have been shown to be promoted by Al^{3+} compounds.[40,41]

In summary, we report the reactions of a low-valent aluminium(I) reagent with a series of aryl methyl ethers to form aluminium building blocks containing polar Al–C and Al–O bonds. In the absence of a catalyst, selective functionalisation of sp^3 C–O bonds occurs in preference to the sp^2 C–O bond. In the presence of catalytic $[Pd(PCy_3)_2]$ there is a complete switch in selectivity for functionalisation of sp^2 C–O bonds. DFT calculations in combination with measurements of KIEs support a pathway involving the ligand-assisted oxidative addition of the sp^2 C–O bond of the substrate to a known Pd–Al intermetallic intermediate. Catalyst switching of chemoselectivity provides access to isomeric organoaluminium building blocks from a single starting material. The new methodology was applied to upgrading a derivative of vanillin.

We are grateful to the European Research Council for and ERC StG (FluoroFix:677367) and Marie Curie Fellowship to F. R. Johnson Matthey are thanked for generous donation of $PdCl_2$. P. J. C. thanks Fundação para a Ciência e a Tecnologia (FCT), Portugal, for projects UIDB/04046/2020, UIDP/04046/2020 (BioISI). P. J. C. also acknowledges Programa Operacional Regional de Lisboa (Lisboa 2020), Portugal 2020, FEDER/FN, and the European Union for project number 28455 (LISBOA-01-0145-FEDER-028455, PTDC/QUI-QFI/28455/2017).

Conflicts of interest

There are no conflicts to declare.

Notes and references

§ A small impurity was detected during the reaction of anisole which was removed in the recrystallisation process. This by-product was identified as the result of C–H alumination of the meta position of anisole and estimated to form in $<5\%$ yield. This minor component is enriched on recrystallisation of **4a**.

1 A. J. Ragauskas, *Science*, 2006, **311**, 484–489.
2 Y. Pu, D. Zhang, P. M. Singh and A. J. Ragauskas, *Biofuels, Bioprod. Biorefin.*, 2008, **2**, 58–73.
3 J. Zakzeski, P. C. A. Bruijnincx, A. L. Jongerius and B. M. Weckhuysen, *Chem. Rev.*, 2010, **110**, 3552–3599.
4 Z. Sun, B. Fridrich, A. de Santi, S. Elangovan and K. Barta, *Chem. Rev.*, 2018, **118**, 614–678.
5 Z. Sun, G. Bottari, A. Afanasenko, M. C. A. Stuart, P. J. Deuss, B. Fridrich and K. Barta, *Nat. Catal.*, 2018, **1**, 82–92.
6 Y. Xin, Y. Jing, L. Dong, X. Liu, Y. Guo and Y. Wang, *Chem. Commun.*, 2019, **55**, 9391–9394.
7 X. Shen, Q. Meng, Q. Mei, H. Liu, J. Yan, J. Song, D. Tan, B. Chen, Z. Zhang, G. Yang and B. Han, *Chem. Sci.*, 2020, **11**, 1347–1352.
8 M. Fache, B. Boutevin and S. Caillol, *ACS Sustainable Chem. Eng.*, 2015, **4**, 35–46.
9 E. Wenkert, E. L. Michelotti and S. C. Swindell, *J. Am. Chem. Soc.*, 1979, **101**, 2246–2247.
10 C. Zarate and R. Martin, *J. Am. Chem. Soc.*, 2014, **136**, 2236–2239.
11 R. J. Somerville, L. V. A. Hale, E. Gómez-Bengoa, J. Bures and R. Martin, *J. Am. Chem. Soc.*, 2018, **140**, 8771–8780.
12 C. Zarate, M. Nakajima and R. Martin, *J. Am. Chem. Soc.*, 2017, **139**, 1191–1197.
13 Y. Gu and R. Martin, *Angew. Chem., Int. Ed.*, 2017, **56**, 3187–3190.
14 H. Kinuta, M. Tobisu and N. Chatani, *J. Am. Chem. Soc.*, 2015, **137**, 1593–1600.
15 C. Zarate, R. Manzano and R. Martin, *J. Am. Chem. Soc.*, 2015, **137**, 6754–6757.
16 R. Seki, N. Hara, T. Saito and Y. Nakao, *J. Am. Chem. Soc.*, 2021, **143**, 6388–6394.
17 S. J. Blanksby and G. B. Ellison, *Acc. Chem. Res.*, 2003, **36**, 255–263.
18 S. Yow, A. E. Nako, L. Neveu, A. J. P. White and M. R. Crimmin, *Organometallics*, 2013, **32**, 5260–5262.
19 M. R. Crimmin, M. J. Butler and A. J. P. White, *Chem. Commun.*, 2015, **51**, 15994–15996.
20 T. N. Hooper, R. K. Brown, F. Rekhroukh, M. Garçon, A. J. P. White, P. J. Costa and M. R. Crimmin, *Chem. Sci.*, 2020, **11**, 7850–7857.
21 C. Cui, H. W. Roesky, H.-G. Schmidt, M. Noltemeyer, H. Hao and F. Cimpoesu, *Angew. Chem., Int. Ed.*, 2000, **39**, 4274–4276.
22 M. Zhong, S. Sinhababu and H. W. Roesky, *Dalton Trans.*, 2020, **49**, 1351–1364.
23 T. Chu, Y. Boyko, I. Korobkov and G. I. Nikonov, *Organometallics*, 2015, **34**, 5363–5365.
24 J. Hicks, P. Vasko, A. Heilmann, J. M. Goicoechea and S. Aldridge, *Angew. Chem., Int. Ed.*, 2020, **59**, 20376–20380.
25 S. Kurumada, K. Sugita, R. Nakano and M. Yamashita, *Angew. Chem., Int. Ed.*, 2020, **59**, 20381–20384.
26 A. Bondi, *J. Phys. Chem.*, 1964, **68**, 441–451.
27 F. Rekhroukh, W. Chen, R. K. Brown, A. J. P. White and M. R. Crimmin, *Chem. Sci.*, 2020, **11**, 7842–7849.
28 T. N. Hooper, M. Garçon, A. J. P. White and M. R. Crimmin, *Chem. Sci.*, 2018, **9**, 5435–5440.
29 W. Chen, T. N. Hooper, J. Ng, A. J. P. White and M. R. Crimmin, *Angew. Chem., Int. Ed.*, 2017, **56**, 12687–12691.
30 B.-T. Guan, S.-K. Xiang, B.-Q. Wang, Z.-P. Sun, Y. Wang, K.-Q. Zhao and Z.-J. Shi, *J. Am. Chem. Soc.*, 2008, **130**, 3268–3269.
31 N. A. Jasim, A. C. Whitwood, A. Lledós, R. N. Perutz and M. A. Ortuño, *Dalton Trans.*, 2016, **45**, 18842–18850.
32 M. E. van der Boom, S.-Y. Liou, Y. Ben-David, L. J. W. Shimon and D. Milstein, *J. Am. Chem. Soc.*, 1998, **120**, 6531–6541.
33 Z. Li, S.-L. Zhang, Y. Fu, Q.-X. Guo and L. Liu, *J. Am. Chem. Soc.*, 2009, **131**, 8815–8823.
34 K. W. Quasdorf, A. Antoft-Finch, P. Liu, A. L. Silberstein, A. Komaromi, T. Blackburn, S. D. Ramgren, K. N. Houk, V. Snieckus and N. K. Garg, *J. Am. Chem. Soc.*, 2011, **133**, 6352–6363.
35 M. C. Schwarzer, R. Konno, T. Hojo, A. Ohtsuki, K. Nakamura, A. Yasutome, H. Takahashi, T. Shimasaki, M. Tobisu, N. Chatani and S. Mori, *J. Am. Chem. Soc.*, 2017, **139**, 10347–10358.
36 S. A. Macgregor, D. C. Roe, W. J. Marshall, K. M. Bloch, V. I. Bakhmutov and V. V. Grushin, *J. Am. Chem. Soc.*, 2005, **127**, 15304–15321.
37 A. L. Raza, J. A. Panetier, M. Teltewskoi, S. A. Macgregor and T. Braun, *Organometallics*, 2013, **32**, 3795–3807.
38 M. Teltewskoi, J. A. Panetier, S. A. Macgregor and T. Braun, *Angew. Chem., Int. Ed.*, 2010, **49**, 3947–3951.
39 C. Wu, S. P. McCollom, Z. Zheng, J. Zhang, C.-C. Sha, M. Li, P. J. Walsh and N. C. Tomson, *ACS Catal.*, 2020, **10**, 7934–7944.
40 P. Kelley, G. A. Edouard, S. Lin and T. Agapie, *Chem. – Eur. J.*, 2016, **22**, 17173–17176.
41 X. Liu, C.-C. Hsiao, I. Kalvet, M. Leiendecker, L. Guo, F. Schoenebeck and M. Rueping, *Angew. Chem., Int. Ed.*, 2016, **55**, 6093–6098.

